13
GRANULAR FLOWS

13.1 INTRODUCTION

Dense fluid-particle flows in which the direct particle-particle interactions are a dominant feature encompass a diverse range of industrial and geophysical contexts (Jaeger *et al.* 1996) including, for example, slurry pipelines (Shook and Roco 1991), fluidized beds (Davidson and Harrison 1971), mining and milling operations, ploughing (Weighardt 1975), abrasive water jet machining, food processing, debris flows (Iverson 1997), avalanches (Hutter 1993), landslides, sediment transport and earthquake-induced soil liquefaction. In many of these applications, stress is transmitted both by shear stresses in the fluid and by momentum exchange during direct particle-particle interactions. Many of the other chapters in this book analyse flow in which the particle concentration is sufficiently low that the particle-particle momentum exchange is negligible.

In this chapter we address those circumstances, usually at high particle concentrations, in which the direct particle-particle interactions play an important role in determining the flow properties. When those interactions dominate the mechanics, the motions are called *granular flows* and the flow patterns can be quite different from those of conventional fluids. An example is included as figure 13.1 which shows the downward flow of sand around a circular cylinder. Note the *upstream wake* of stagnant material in front of the cylinder and the empty cavity behind it.

Within the domain of granular flows, there are, as we shall see, several very different types of flow distinguished by the fraction of time for which particles are in contact. For most slow flows, the particles are in contact most of the time. Then large transient structures or assemblages of particles known as *force chains* dominate the rheology and the inertial effects of the random motions of individual particles play little role. Force chains are ephemeral,

Figure 13.1. Long exposure photograph of the downward flow of sand around a circular cylinder. Reproduced with the permission of R.H.Sabersky.

quasi-linear sequences of particles with large normal forces at their contact points. They momentarily carry much of the stress until they buckle or are superceded by other chains. Force chains were first observed experimentally by Drescher and De Josselin de Jong (1972) and, in computer simulations, by Cundall and Strack (1979).

13.2 PARTICLE INTERACTION MODELS

It is self-evident that the rheology of granular flows will be strongly influenced by the dynamics of particle-particle interactions. Consequently the solid mechanics and dynamics of those interactions must be established prior to a discussion of the rheology of the overall flow. We note that the relation between the rheology and the particle-particle interaction can quite subtle (Campbell 2002, 2003).

Early work on rapid granular material flows often assumed instantaneous,

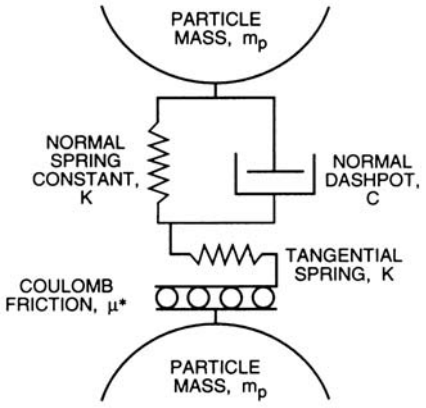

Figure 13.2. Schematic of the soft particle model of particle interaction.

binary collisions between particles, in other words a *hard particle model* (see, for example, Campbell and Brennen 1985a, b). While this assumption may be valid in some applications, it is now recognized that the high shear rates required to achieve such flow conditions are unusual (Campbell 2002) and that most practical granular flows have more complex particle-particle interactions that, in turn, lead to more complex rheologies. To illustrate this we will confine the discussion to the particular form of particle-particle interaction most often used in computer simulations. We refer to the model of the particle-particle dynamics known as the *soft particle model*, depicted in figure 13.2. First utilized by Cundall and Strack (1979), this admittedly simplistic model consists of a spring, K_n, and dashpot, C, governing the normal motion and a spring, K_s, and Coulomb friction coefficient, μ^*, governing the tangential motion during the contact and deformation of two particles of mass, m_p. The model has been subject to much study and comparison with experiments, for example by Bathurst and Rothenburg (1988). Though different normal and tangential spring constants are often used we will, for simplicity, characterize them using a single spring constant (Bathurst and Rothenburg show that K_s/K_n determines the bulk Poisson's ratio) that, neglecting the effects of non-linear Hertzian-like deformations will be characterized by a simple linear elastic spring constant, K. Note that as described by Bathurst and Rothenburg, the Young's modulus of the bulk material will be proportional to K. Note also that K will be a function not only of properties of the solid material but also of the geometry of the contact points. Furthermore, it is clear that the dashpot constant, C, will determine the loss of energy during normal collisions and will therefore be directly related to the coefficient of restitution for normal collisions. Consequently, appro-

priate values of C can be determined from known or measured coefficients of restitution, ϵ; the specific relation is

$$\epsilon = exp\left(-\pi C/\left[2m_pK - C^2\right]^{\frac{1}{2}}\right) \tag{13.1}$$

Note that this particle interaction model leads to a collision time for individual binary collisions, t_c, that is the same for all collisions and is given by

$$t_c = \pi m_p/\left[2m_pK - C^2\right]^{\frac{1}{2}} \tag{13.2}$$

Before leaving the subject of individual particle interactions, several cautionary remarks are appropriate. Models such as that described above and those used in most granular flow simulations are highly simplified and there are many complications whose effects on the granular flow rheology remain to be explored. For example, the spring stiffnesses and the coefficients of restitution are often far from constant and depend on the geometry of the particle-particle contacts and velocity of the impact as well as other factors such as the surface roughness. The contact stiffnesses may be quite non-linear though Hertzian springs (in which the force is proportional to the displacement raised to the 3/2 power) can be readily incorporated into the computer simulations. We also note that velocities greater than a few cm/s will normally lead to plastic deformation of the solid at the contact point and to coefficients of restitution that decrease with increasing velocity (Goldsmith 1960, Lun and Savage 1986). Boundary conditions may also involve complications since the coefficient of restitution of particle-wall collisions can depend on the wall thickness in a complicated way (Sondergard *et al.* 1989). Appropriate tangential coefficients are even more difficult to establish. The tangential spring stiffness may be different from the normal stiffness and may depend on whether or not slippage occurs during contact. This introduces the complications of tangential collisions studied by Maw *et al.*(1976, 1981), Foerster *et al.*(1994) and others. The interstitial fluid can have a major effect on the interaction dynamics; further comment on this is delayed until section 13.6. The point to emphasize here is that much remains to be done before all the possible effects on the granular flow rheology have been explored.

13.2.1 Computer simulations

Computer simulations have helped to elucidate the behavior of all types of granular flow. They are useful for two reasons. First there is a dearth

of experimental techniques that would allow complete observations of real granular flows and their flow variables such as the local solids fraction; this is particularly the case for interior regions of the flow. Second, it is useful to be able to simplify the particle-particle and particle-wall interactions and therefore learn the features that are most important in determining the flow. The simulations use both *hard particle* models (see, for example, Campbell and Brennen 1985a, b) and *soft particle* models (see, for example, Cundall and Strack (1979), Walton and Braun 1986a, b). The hard particle model is, of course, a limiting case within the soft particle models and, though computationally efficient, is only applicable to rapid granular flows (see section 13.5). Soft particle models have been particularly useful in helping elucidate granular material flow phenomena, for example the formation and dissipation of force chains (Cundall and Strack 1979) and the complex response of a bed of grains to imposed vertical vibration (Wassgren *et al.* 1996).

13.3 FLOW REGIMES

13.3.1 Dimensional Analysis

As pointed out by Campbell (2002), given a particle interaction model (such as that described above) characterized by a set of parameters like (K, ϵ, μ^*), it follows from dimensional analysis that the stress, τ, in a typical shearing flow with a shear rate, $\dot{\gamma}$, and a solids volume fraction, α, will be a function of the particle interaction parameters plus $(D, \rho_S, \alpha, \dot{\gamma})$ where the particle density ρ_S has been used instead of the particle mass, m_p. Applying dimensional analysis to this function it follows that the dimensionless stress, $\tau D/K$, must be a function of the following dimensionless quantities:

$$\frac{\tau D}{K} = f\left(\alpha, \mu^*, \epsilon, \frac{K}{\rho_S D^3 \dot{\gamma}^2}\right) \tag{13.3}$$

Alternatively one could also use a different form for the non-dimensional stress, namely $\tau/\rho_S D^2 \dot{\gamma}^2$, and express this as a function of the same set of dimensionless quantities.

Such a construct demonstrates the importance in granular flows of the parameter, $K/\rho_S D^3 \dot{\gamma}^2$, which is the square of the ratio of the typical time associated with the shearing, $t_{shear} = 1/\dot{\gamma}$, to a typical collision time, $(m_p/K)^{\frac{1}{2}}$. The shearing time, t_{shear}, will determine the time between collisions for a particular particle though this time will also be heavily influenced by the solids fraction, α. The typical collision time, $(m_p/K)^{\frac{1}{2}}$, will be close to the binary collision time. From these considerations, we can discern two possible

flow regimes or asymptotic flow states. The first is identified by instantaneous (and therefore, necessarily binary) collisions in which the collision time is very short compared with the shearing time so that $K/\rho_S D^3\dot{\gamma}^2 \gg 1$. We will we refer to this as the *inertial regime*. It includes an asymptotic case called *rapid granular flows* in which the collisions are essentially instantaneous and binary. The above dimensional analysis shows that appropriate dimensionless stresses in the inertial regime take the form $\tau/\rho_S D^2\dot{\gamma}^2$ and should be functions only of

$$\frac{\tau}{\rho_S D^2\dot{\gamma}^2} = f\left(\alpha, \mu^*, \epsilon\right) \tag{13.4}$$

This is the form that Bagnold (1954) surmised in his classic and much quoted paper on granular shear flows.

The second asymptotic flow regime is characterized by contact times that are long compared with the shearing time so that $K/\rho_S D^3\dot{\gamma}^2 \ll 1$. From computer simulations Campbell (2002) finds that as $K/\rho_S D^3\dot{\gamma}^2$ is decreased and the flow begins to depart from the inertial regime, the particles are forced to interact with a frequency whose typical time becomes comparable to the binary collision time. Consequently multiple particle interactions begin to occur and force chains begin to form. Then the dimensional analysis shows that the appropriate dimensionless stresses are $\tau D/K$ and, in this limit, these should only be functions of

$$\frac{\tau D}{K} = f\left(\alpha, \mu^*, \epsilon\right) \tag{13.5}$$

Note that this second regime is essentially quasistatic in that the stresses do not depend on any rate quantities. Campbell refers to this as the elastic-quasistatic regime.

13.3.2 Flow regime rheologies

Campbell (2002, 2003) has carried out an extensive series of computer simulations of shear flows designed to identify further characteristics of the flow regimes and, in particular, to identify the boundaries between them. Though his results are complicated because the simulations carried out with the solids fraction fixed seem to exhibit differences from those carried out with the normal stress or overburden fixed, we give here a brief overview of a few key features and results emerging from the fixed normal stress simulations. As one might expect, the flows at low values of $K/\rho_S D^3\dot{\gamma}^2$ are dominated by force chains that carry most of the shear stress in the shear flow. These chains form, rotate and disperse continually during shear (Drescher

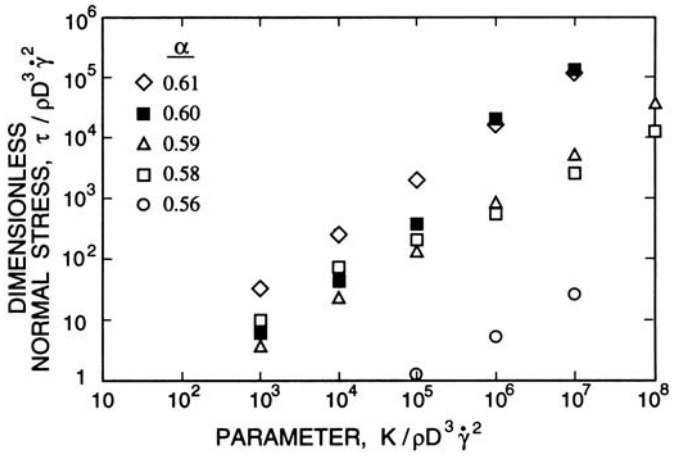

Figure 13.3. Typical non-dimensional stress, $\tau/\rho_S D^2\dot{\gamma}^2$ (in this case a normal stress) in a uniform shear flow as a function of the parameter, $K/\rho_S D^3\dot{\gamma}^2$, for various solids fractions, α, a friction coefficient $\mu^* = 0.5$ and a coefficient of restitution of $\epsilon = 0.7$ (adapted from Campbell 2003).

and De Josselin de Jong 1972, Cundall and Strack 1979). Evaluating the typical particle contact time, Campbell finds that, in this elastic-quasistatic regime the dynamics are not correlated with the binary contact time but are determined by the shear rate. This clearly indicates multiple particle structures (force chains) whose lifetime is determined by their rotation under shear. However, as $K/\rho_S D^3\dot{\gamma}^2$ is increased and the flow approaches the rapid granular flow limit, the typical contact time asymptotes to the binary contact time indicating the dominance of simple binary collisions and the disappearance of force chains.

Figure 13.3 is a typical result from Campbell's simulations at fixed normal stress and plots the dimensionless stress $\tau/\rho_S D^2\dot{\gamma}^2$ against the parameter $K/\rho_S D^3\dot{\gamma}^2$ for various values of the solids fraction, α. Note that at high solids fractions the slopes of the curves approach unity indicating that the ratio, $\tau D/K$, is constant in that part of the parameter space. This is therefore the elastic-quasistatic regime. At lower solids fractions, the dimensionless stress is a more complex function of both solids fraction and the parameter, $K/\rho_S D^3\dot{\gamma}^2$, thus indicating the appearance of inertial effects. Another interesting feature is the ratio of the shear to normal stress, τ_s/τ_n, and the manner in which it changes with the change in flow regime. At high $K/\rho_S D^3\dot{\gamma}^2$ this ratio asymptotes to a constant value that corresponds to the internal friction angle used in soil mechanics (and is closely related to the interparticle friction coefficient, μ^*). However, as $K/\rho_S D^3\dot{\gamma}^2$ is decreased

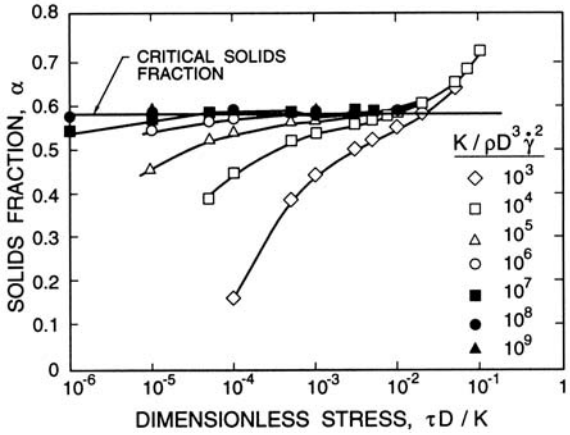

Figure 13.4. The variation of the solids fraction, α, with the dimensionless applied stress, $\tau D/K$, in a uniform shear flow with fixed normal stress for various values of the parameter, $K/\rho_S D^3\dot{\gamma}^2$. Computer simulation data from Campbell (2003) for the case of a friction coefficient of $\mu^* = 0.5$ and a coefficient of restitution of $\epsilon = 0.7$.

(at constant normal stress) the simulations show τ_s/τ_n increasing with the increases being greater the smaller the normal stress.

Fundamental rheological information such as given in figure 13.3 can be used to construct granular flow regime maps. However, it is first necessary to discuss the solids fraction, α, and how that is established in most granular flows. The above analysis assumed, for convenience, that α was known and sought expressions for the stresses, τ, both normal and tangential. In practical granular flows, the normal stress or overburden is usually established by the circumstances of the flow and by the gravitational forces acting on the material. The solids fraction results from the rheology of the flow. Under such circumstances, the data required is the solids fraction, α as a function of the dimensionless overburden, $\tau D/K$ for various values of the parameter, $K/\rho_S D^3\dot{\gamma}^2$. An example from Campbell (2003), is shown in figure 13.4 and illustrates another important feature of granular dynamics. At high values of the overburden and solids fraction, the rate parameter, $K/\rho_S D^3\dot{\gamma}^2$ plays little role and the solids fraction simply increases with the overburden. As the solids fraction decreases in order to facilitate flow, then, for low shear rates or high values of $K/\rho_S D^3\dot{\gamma}^2$, the material asymptotes to a *critical* solids fraction of about 0.59 in the case of figure 13.4. This is the critical state phenomenon familiar to soil mechanicists (see, for example, Schofield and Wroth 1968). However, at higher shear rates, lower values of $K/\rho_S D^3\dot{\gamma}^2$, and lower overburdens, the material expands below the critical

solids fraction as the material moves into the inertial regime and the collisions and interactions between the particles cause the material to expand. Figure 13.4 therefore displays both the traditional soil mechanics behavior and the classic kinetic theory behavior that results from the dominance of random, collisional motions. We also see that the traditional critical solids fraction could be considered as the dividing line between the inertial and elastic-quasistatic regimes of flow.

13.3.3 Flow regime boundaries

Finally, we include as figure 13.5, a typical flow regime map as constructed by Campbell (2003) from this computer-modeled rheological information. The regimes are indicated in a map of the overburden or dimensionless stress plotted against the parameter $K/\rho_S D^3\dot{\gamma}^2$ and the results show the progression at fixed overburden from the elastic-quasistatic regime at low shear rates to the inertial regime. Campbell also indicates that part of the inertial regime in which the flow is purely collisional (rapid granular flow). This occurs at low overburdens but at sufficiently high shear rates that rapid granular flows are uncommon in practice though they have been generated in a number of experimental shear cell devices.

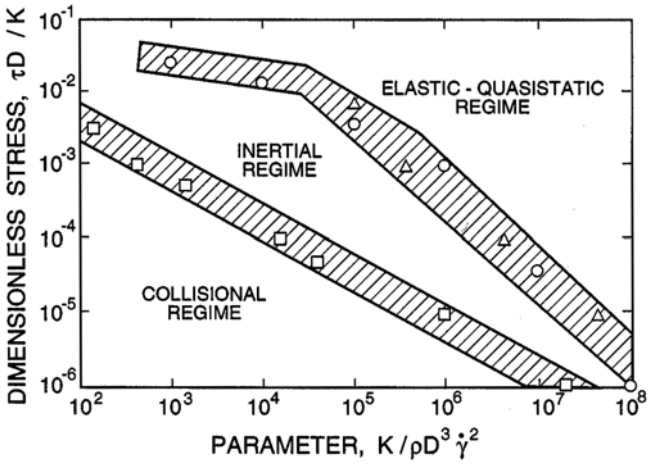

Figure 13.5. Typical flow regime map for uniform shear flow in a plot of the dimensionless overburden or normal stress against the parameter, $K/\rho_S D^3\dot{\gamma}^2$, as determined from the fixed normal stress computer simulations of Campbell (2003) (for the case of a friction coefficient of $\mu^* = 0.5$ and a coefficient of restitution of $\epsilon = 0.7$).

13.4 SLOW GRANULAR FLOW

13.4.1 Equations of motion

All of the early efforts to understand granular flow neglected the random kinetic energy of the particles, the granular temperature, and sought to construct equations for the motion as extrapolations of the theories of soil mechanics by including the mean or global inertial effects in the equations of motion. We now recognize that, if these constructs are viable, they apply to the elastic-quasistatic regime of slow granular motion. Notable among these theories were those who sought to construct effective continuum equations of motion for the granular material beginning with

$$\frac{D(\rho_S \alpha)}{Dt} + \rho_S \alpha \frac{\partial u_i}{\partial x_i} = 0 \tag{13.6}$$

$$\rho_S \alpha \frac{Du_k}{Dt} = \rho_S \alpha g_k - \frac{\partial \sigma_{ki}}{\partial x_i} \tag{13.7}$$

where equation 13.6 is the continuity equation 1.25 and equation 13.7 is the momentum equation (equation 1.46 for a single phase flow). It is then assumed that the stress tensor is quasistatic and determined by conventional soil mechanics constructs. A number of models have been suggested but here we will focus on the most commonly used approach, namely Mohr-Coulomb models for the stresses.

13.4.2 Mohr-Coulomb models

As a specific example, the Mohr-Coulomb-Jenike-Shield model (Jenike and Shield 1959) utilizes a Mohr's circle diagram to define a yield criterion and it is assumed that once the material starts to flow, the stresses must continue to obey that yield criterion. For example, in the flow of a cohesionless material, one might utilize a Coulomb friction yield criterion in which it is assumed that the ratio of the principal shear stress to the principal normal stress is simply given by the *internal friction angle*, ϕ, that is considered to be a material property. In a two-dimensional flow, for example, this would imply the following relation between the stress tensor components:

$$\left\{ \left(\frac{\sigma_{xx} - \sigma_{yy}}{2} \right)^2 + \sigma_{xy}^2 \right\}^{\frac{1}{2}} = -sin\phi \left(\frac{\sigma_{xx} + \sigma_{yy}}{2} \right) \tag{13.8}$$

where the left hand side would be less than the right in regions where the material is not flowing or deforming.

However, equations 13.6, 13.7, and 13.8, are insufficient and must be supplemented by at least two further relations. In the Mohr-Coulomb-Jenike-Shield model, an assumption of isotropy is also made; this assumes that the directions of principal stress and principal strain rate correspond. For example, in two-dimensional flow, this implies that

$$\frac{\sigma_{xx} - \sigma_{yy}}{\sigma_{xy}} = \frac{2\left(\frac{\partial u}{\partial x} - \frac{\partial v}{\partial y}\right)}{\frac{\partial u}{\partial y} + \frac{\partial v}{\partial x}} \tag{13.9}$$

It should be noted that this part of the model is particularly suspect since experiments have shown substantial departures from isotropy. Finally one must also stipulate some relation for the solids fraction α and typically this has been considered a constant equal to the critical solids fraction or to the maximum shearable solids fraction. This feature is also very questionable since even slow flows such as occur in hoppers display substantial decreases in α in the regions of faster flow.

13.4.3 Hopper flows

Despite the above criticisms, Mohr-Coulomb models have had some notable successes particularly in their application to flows in hoppers. Savage (1965, 1967), Morrison and Richmond (1976), Brennen and Pearce (1978), Nguyen *et al.*(1979), and others utilized Mohr-Coulomb models (and other variants) to find approximate analytical solutions for the flows in hoppers, both conical hoppers and two-dimensional hopper flows. Several types of hopper are

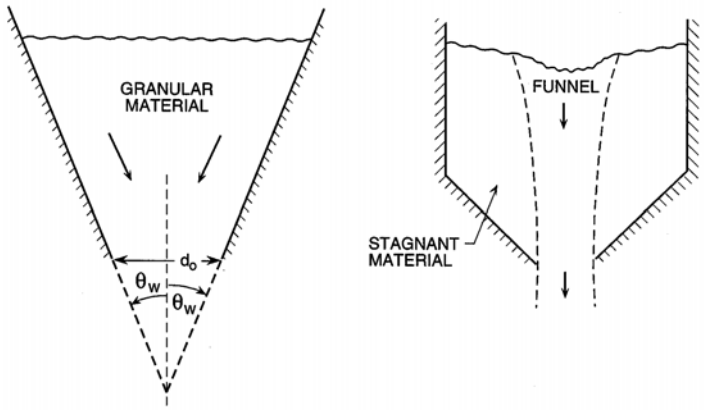

Figure 13.6. Some hopper geometries and notation. Left: a mass flow hopper. Right: funnel flow.

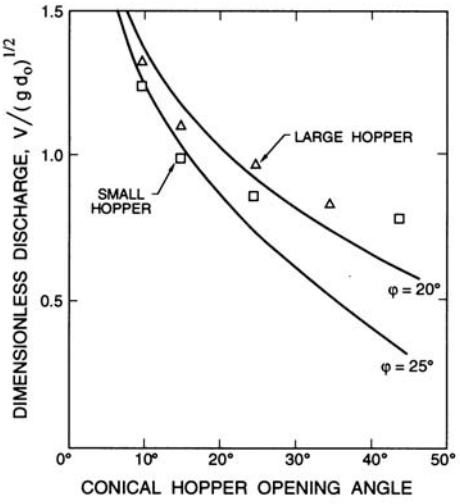

Figure 13.7. Dimensionless discharge, $V/(gd_o)^{\frac{1}{2}}$ (d_o is the opening width and V is the volume-averaged opening velocity), for flows in conical hoppers of various hopper opening angles, θ_w. Experimental data for the flows of glass beads (internal friction angle, $\phi = 25^o$, wall friction angle of 15^o) in two sizes of hopper are compared with the Mohr-Coulomb-Jenike-Shield calculations of Nguyen *et al.*(1979) using internal friction angles of 20^o and 25^o.

shown in figure 13.6. In narrow *mass flow* hoppers with small opening angles, θ_w, these solutions yield flow rates that agree well with the experimentally measured values for various values of θ_w, various internal friction angles and wall friction angles. An example of the comparison of calculated and experimental flow rates is included in figure 13.7. These methods also appear to yield roughly the right wall stress distributions. In addition note that both experimentally and theoretically the flow rate becomes independent of the height of material in the hopper once that height exceeds a few opening diameters; this result was explored by Janssen (1895) in one of the earliest papers dealing with granular flow.

Parenthetically, we note even granular flows as superficially simple as flows in hoppers can be internally quite complex. For example, it is only for narrow hoppers that even low friction granular materials manifest *mass flow*. At larger hopper angles and for more frictional materials, only an internal *funnel* of the granular material actually flows (see figure 13.6) and the material surrounding that funnel remains at rest. Funnel flows are of considerable practical interest (see, for example, Jenike 1964, Johanson and Colijin 1964) and a substantial literature exists for the heuristic determination of the con-

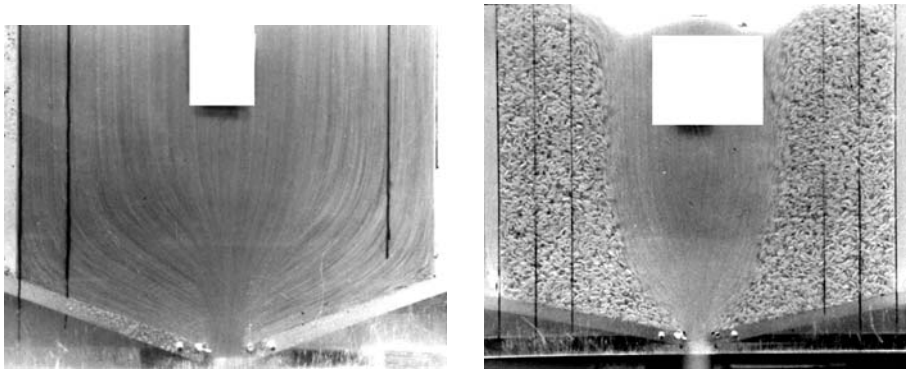

Figure 13.8. Long exposure photographs of typical granular flows in hoppers showing the streamlines in the flowing material. Left: flow of sand without stagnant regions. Right: a funnel flow of rice with stagnant regions. From Nguyen *et al.*(1980).

ditions under which they occur; for a study of the conditions that determine these various flow patterns see Nguyen *et al.*(1980). One interpretation of funnel flow is that the stress state within the funnel is sufficient to allow dilation of the material and therefore flow whereas the surrounding stagnant material has a stress state in which the solids fraction remains above the critical. It should be possible to generate computer simulations of these complex flows that predict the boundaries between the shearing and non-shearing regions in a granular flow. However, it is clear that some of the experimentally observed flows are even more complex than implied by the above description. With some materials the flow can become quite unsteady; for example, Lee *et al.* (1974) observed the flow in a two-dimensional hopper to oscillate from side to side with the alternating formation of yield zones within the material.

13.5 RAPID GRANULAR FLOW

13.5.1 Introduction

Despite the uncommon occurence of truly rapid granular flow, it is valuable to briefly review the substantial literature of analytical results that have been generated in this field. At high shear rates, the inertia of the random motions that result from particle-particle and particle-wall collisions becomes a key feature of the rheology. Those motions can cause a dilation of the material and the granular material begins to behave like a molecular gas. In such a flow, as in kinetic theory, the particle velocities can be

decomposed into time averaged and fluctuating velocity components. The energy associated with the random or fluctuating motions is represented by the granular temperature, T, analogous to the thermodynamic temperature. Various granular temperatures may be defined depending on whether one includes the random energy associated with rotational and vibrational modes as well as the basic translational motions. The basic translational granular temperature used herein is defined as

$$T = \frac{1}{3}\left(< \grave{U}_1^2 > + < \grave{U}_2^2 > + < \grave{U}_3^2 >\right) \tag{13.10}$$

where $\grave{U}_i$ denotes the fluctuating velocity with a zero time average and $< >$ denotes the ensemble average. The kinetic theory of granular material is complicated in several ways. First, instead of tiny point molecules it must contend with a large solids fraction that inhibits the mean free path or flight of the particles. The large particle size also means that momentum is transported both through the flight of the particles (the *streaming* component of the stress tensor) and by the transfer of momentum from the center of one particle to the center of the particle it collides with (the *collisional* component of the stress tensor). Second, the collisions are inelastic and therefore the velocity distributions are not necessarily Maxwellian. Third, the finite particle size means that there may be a significant component of rotational energy, a factor not considered in the above definition. Moreover, the importance of rotation necessarily implies that the communication of rotation from one particle to another may be important and so the tangential friction in particle-particle and particle-wall collisions will need to be considered. All of this means that the development of a practical kinetic theory of granular materials has been long in development.

Early efforts to construct the equations governing rapid granular flow followed the constructs of Bagnold (1954); though his classic experimental observations have recently come under scrutiny (Hunt *et al.* 2002), his qualitative and fundamental understanding of the issues remains valid. Later researchers, building on Bagnold's ideas, used the concept of granular temperature in combination with heuristic but insightful assumptions regarding the random motions of the particles (see, for example, McTigue 1978, Ogawa *et al.* 1980, Haff 1983, Jenkins and Richman 1985, Nakagawa 1988, Babic and Shen 1989) in attempts to construct the rheology of rapid granular flows. Ogawa *et al.* (1978, 1980), Haff (1983) and others suggested that the global shear and normal stresses, τ_s and τ_n, are given by

$$\tau_s = f_s(\alpha)\rho_S\dot{\gamma}T^{\frac{1}{2}} \qquad \text{and} \qquad \tau_n = f_n(\alpha)\rho_S T \tag{13.11}$$

where f_s and f_n are functions of the solid fraction, α, and some properties of the particles. Clearly the functions, f_s and f_n, would have to tend to zero as $\alpha \to 0$ and become very large as α approaches the maximum shearable solids fraction. The constitutive behavior is then completed by some relation connecting T, α and, perhaps, other flow properties. Though it was later realized that the solution of a *granular energy* equation would be required to determine T, early dimensional analysis led to speculation that the granular temperature was just a local function of the shear rate, $\dot{\gamma}$ and that $T^{\frac{1}{2}} \propto D\dot{\gamma}$. With some adjustment in f_s and f_n this leads to

$$\tau_s = f_s(\alpha)\rho_S D^2\dot{\gamma}^2 \qquad \text{and} \qquad \tau_n = f_n(\alpha)\rho_S D^2\dot{\gamma}^2 \tag{13.12}$$

which implies that the effective friction coefficient, τ_s/τ_n should only be a function of α and the particle characteristics.

13.5.2 Example of rapid flow equations

Later, the work of Savage and Jeffrey (1981) and Jenkins and Savage (1983) saw the beginning of a more rigorous application of kinetic theory methods to rapid granular flows and there is now an extensive literature on the subject (see, for example, Gidaspow 1994). The kinetic theories may be best exemplified by quoting the results of Lun *et al.* (1984) who attempted to evaluate both the collisional and streaming contributions to the stress tensor (since momentum is transported both by the collisions of finite-sized particles and by the motions of the particles). In addition to the continuity and momentum equations, equations 13.6 and 13.7, an *energy equation* must be constructed to represent the creation, transport and dissipation of granular heat; the form adopted is

$$\frac{3}{2}\rho_S\alpha\frac{DT}{Dt} = -\frac{\partial q_i}{\partial x_i} + \frac{\partial u_j}{\partial x_i}\sigma_{ji} - \Gamma \tag{13.13}$$

where T is the granular temperature, q_i is the granular heat flux vector, and Γ is the rate of dissipation of granular heat into thermodynamic heat per unit volume. Note that this represents a balance between the granular heat stored in a unit volume (the lefthand side), the conduction of granular heat into the unit volume (first term on RHS), the generation of granular heat (second term on RHS) and the dissipation of granular heat (third term on RHS).

Most of the kinetic theories begin in this way but vary in the expressions obtained for the stress/strain relations, the granular heat flux and the dissipation term. As an example we quote here the results from the kinetic theory

of Lun *et al.* (1984) that have been subsequently used by a number of authors. Lun *et al.* obtain a stress tensor related to the granular temperature, T (equation 13.10), by

$$\sigma_{ij} = \left(\rho_S g_1 T - \frac{4\pi^{\frac{1}{2}}}{3} \rho_S \alpha^2 (1+\epsilon) g_0 T^{\frac{1}{2}} \frac{\partial u_i}{\partial x_i} \right) \delta_{ij}$$

$$-2\rho_S D g_2 T^{\frac{1}{2}} \left(\frac{1}{2}(u_{ij} + u_{ji}) - \frac{1}{3} u_{kk} \delta_{ij} \right) \tag{13.14}$$

an expression for the granular heat flux vector,

$$q_i = -\rho_S D \left(g_3 T^{\frac{1}{2}} \frac{\partial T}{\partial x_i} + g_4 T^{\frac{3}{2}} \frac{\partial \alpha}{\partial x_i} \right) \tag{13.15}$$

and an expression for the rate of dissipation of granular heat,

$$\Gamma = \rho_S g_5 T^{\frac{3}{2}} / D \tag{13.16}$$

where $g_0(\alpha)$, the radial distribution function, is chosen to be

$$g_0 = (1 - \alpha/\alpha^*)^{-2.5\alpha^*} \tag{13.17}$$

and α^* is the maximum shearable solids fraction. In the expressions 13.14, 13.15, and 13.16, the quantities g_1, g_2, g_3, g_4, and g_5, are functions of α and ϵ as follows:

$$g_1(\alpha, \epsilon) = \alpha + 2(1+\epsilon)\alpha^2 g_0$$

$$g_2(\alpha, \epsilon) = \frac{5\pi^{\frac{1}{2}}}{96} \left(\frac{1}{\eta(2-\eta) g_0} + \frac{8(3\eta - 1)\alpha}{5(2-\alpha)} + \frac{64\eta\alpha^2 g_0}{25} \left(\frac{(3\eta - 2)}{(2-\eta)} + \frac{12}{\pi} \right) \right)$$

$$g_3(\alpha, \epsilon) = \frac{25\pi^{\frac{1}{2}}}{16\eta(41 - 33\eta)} \left(\frac{1}{g_0} + 2.4\eta\alpha(1 - 3\eta + 4\eta^2) \right.$$

$$\left. + \frac{16\eta^2\alpha^2 g_0}{25} \left(9\eta(4\eta - 3) + 4(41 - 33\eta)/\pi \right) \right)$$

$$g_4(\alpha, \epsilon) = \frac{15\pi^{\frac{1}{2}}(2\eta - 1)(\eta - 1)}{4(41 - 33\eta)} \left(\frac{1}{\alpha g_0} + 2.4\eta \right) \frac{d}{d\alpha}(\alpha^2 g_0)$$

$$g_5(\alpha, \epsilon) = \frac{48\eta(1-\eta)\alpha^2 g_0}{\pi^{\frac{1}{2}}} \tag{13.18}$$

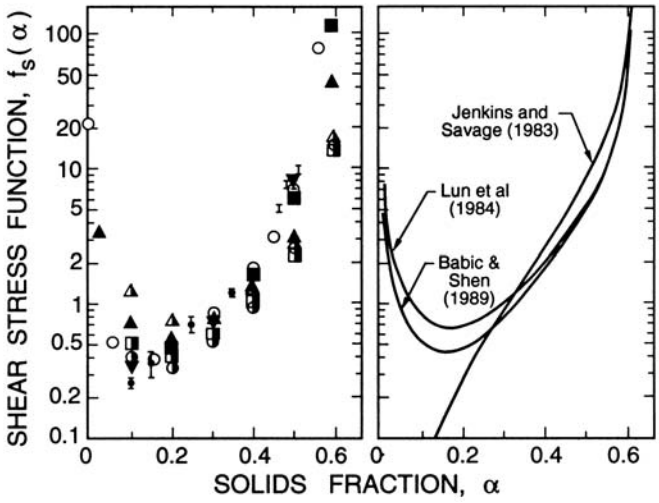

Figure 13.9. Left: the shear stress function, $f_s(\alpha)$, from the experiments of Savage and Sayed (1984) with glass beads (symbol I) and various computer simulations (open symbols: with hard particle model; solid symbols: with soft particle model; half solid symbols: with Monte Carlo methods). Right: Several analytical results. Adapted from Campbell (1990).

where $\eta = (1+\epsilon)/2$.

For two-dimensional shear flows in the (x, y) plane with a shear $\partial u/\partial y$ and no acceleration in the x direction the Lun *et al.* relations yield stresses given by:

$$\sigma_{xx} = \sigma_{yy} = \rho_S g_1 T \quad ; \quad \sigma_{xy} = -\rho_S D g_2 T^{\frac{1}{2}} \frac{\partial u}{\partial y} \tag{13.19}$$

in accord with the expressions 13.11. They also yield a granular heat flux component in the y direction given by:

$$q_y = \rho_S D \left(g_3 T^{\frac{1}{2}} \frac{\partial T}{\partial y} + g_4 T^{\frac{3}{2}} \frac{\partial \alpha}{\partial y} \right) \tag{13.20}$$

These relations demonstrate the different roles played by the quantities g_1, g_2, g_3, g_4, and g_5: g_1 determines the normal kinetic pressure, g_2 governs the shear stress or *viscosity*, g_3 and g_4 govern the diffusivities controlling the conduction of granular heat from regions of differing temperature and density and g_5 determines the granular dissipation. While other kinetic theories may produce different specific expressions for these quantities, all of them seem necessary to model the dynamics of a rapid granular flow.

Figure 13.9 shows typical results for the shear stress function, $f_s(\alpha)$. The lefthand graph includes the data of Savage and Sayed (1984) from shear

cell experiments with glass beads as well as a host of computer simulation results using both hard and soft particle models and both mechanistic and Monte Carlo methods. The righthand graph presents some corresponding analytical results. The stress states to the left of the minima in these figures are difficult to observe experimentally, probably because they are unstable in most experimental facilities.

In summary, the governing equations, exemplified by equations 13.6, 13.7 and 13.13 must be solved for the unknowns, α, T and the three velocity components, u_i given the expressions for σ_{ij}, q_i and Γ and the physical constants D, ρ_S, ϵ, α^* and gravity g_k.

It was recognized early during research into rapid granular flows that some modification to the purely collisional kinetic theory would be needed to extend the results towards lower shear rates at which frictional stresses become significant. A number of authors explored the consequences of heuristically adding frictional terms to the collisional stress tensor (Savage 1983, Johnson *et al.*, 1987, 1990) though it is physically troubling to add contributions from two different flow regimes.

13.5.3 Boundary conditions

Rheological equations like those given above, also require the stipulation of appropriate boundary conditions and it transpires this is a more difficult issue than in conventional fluid mechanics. Many granular flows change quite drastically with changes in the boundary conditions. For example, the shear cell experiments of Hanes and Inman (1985) yielded stresses about three times those of Savage and Sayed (1984) in a very similar apparatus; the modest differences in the boundary roughnesses employed seem to be responsible for this discrepancy. Moreover, computer simulations in which various particle-wall interaction models have been examined (for example, Campbell and Brennen, 1985a,b) exhibit similar sensitivities. Though the normal velocity at a solid wall must necessarily be zero, the tangential velocities may be non-zero due to wall slip. Perhaps a Coulomb friction condition on the stresses is appropriate. But one must also stipulate a wall boundary condition on the granular temperature and this is particularly complicated for wall slip will imply that work is being done by the wall on the granular material so that the wall is a source of granular heat. At the same time, the particle-wall collisions dissipate energy; so the wall could be either a granular heat source or sink. The reader is referred to the work of Hui *et al.* (1984), Jenkins and Richman (1986), Richman (1988) and Campbell (1993) for further discussion of the boundary conditions.

13.5.4 Computer simulations

Computer simulations have helped to elucidate the rheology of rapid granular flows and allowed evaluation of some of the approximations inherent in the theoretical kinetic theory models. For example, the shape of the fluctuation velocity distributions begins to deviate from Maxwellian and the velocity fluctuations become more and more non-isotropic as the solids fraction approaches the maximum shearable value. These kinds of details require computer simulations and were explored, for example in the *hard particle* simulations of shear and chute flows by Campbell and Brennen (1985a,b). More generally, they represent the kinds of organized microstructure that can characterize granular flows close to the maximum shearable solids fraction. Campbell and Brennen (1985a) found that developing microstructure could be readily detected in these shear flow simulations and was manifest in the angular distribution of collision orientations within the shear flow. It is also instructive to observe other phenomenon in the computer simulations such as the conduction of granular temperature that takes place near the bed of a chute flow and helps establish the boundary separating a shearing layer of subcritical solids fraction from the non-shearing, high solids fraction block riding on top of that shearing layer (Campbell and Brennen, 1985b).

13.6 EFFECT OF INTERSTITIAL FLUID

13.6.1 Introduction

All of the above analysis assumed that the effect of the interstitial fluid was negligible. When the fluid dynamics of the interstitial fluid have a significant effect on the granular flow, analysis of the rheology becomes even more complex and our current understanding is quite incomplete. It was Bagnold (1954) who first attempted to define those circumstances in which the interstitial fluid would begin to effect the rheology of a granular flow. Bagnold introduced a parameter that included the following dimensionless quantity

$$Ba = \rho_S D^2 \dot{\gamma} / \mu_L \tag{13.21}$$

where $\dot{\gamma}$ is the shear rate; we will refer to Ba as the Bagnold number. It is simply a measure of the stresses communicated by particle-particle collisions (given according to kinetic theory ideas by $\rho_S V^2$ where V is the typical random velocity of the particles that, in turn, is estimated to be given by $V = D\dot{\gamma}$) to the viscous stress in the fluid, $\mu_L \dot{\gamma}$. Bagnold concluded that when the value of Ba was less than about 40, the viscous fluid stresses dominate and the mixture exhibits a Newtonian rheology in which the shear

stress and the strain rate ($\dot{\gamma}$) are linearly related; he called this the viscous regime. On the other hand when Ba is greater than about 400, the direct particle-particle (and particle-wall) interactions dominate and the stresses become proportional to the square of the strain rate. The viscous regime can be considered the dense suspension regime and many other sections of this book are relevant to those circumstances in which the direct particle-particle and particle-wall interactions play a minor role in the mixture rheology. In this chapter we have focused attention on the other limit in which the effect of the interstitial fluid is small and the rheology is determined by the direct interactions of the particles with themselves and with the walls.

13.6.2 Particle collisions

A necessary prerequisite for the understanding of interstitial fluid effects on granular material flows is the introduction of interstitial fluid effects into particle/particle interaction models such as that described in section 13.2. But the fluid mechanics of two particles colliding in a viscous fluid is itself a complicated one because of the coupling between the intervening lubrication layer of fluid and the deformation of the solid particles (Brenner 1961, Davis *et al.* 1986, Barnocky and Davis 1988). Joseph *et al.*(2001) have recently accumulated extensive data on the coefficient of restitution for spheres (diameter, D, and mass, m_p) moving through various liquids and gases to collide with a solid wall. As demonstrated in figure 13.10, this data shows that the coefficient of restitution for collision normal to the wall is primarily a function of the Stokes number, St, defined as $St = 2m_pV/3\pi\mu D^2$ where μ is the viscosity of the suspending fluid and V is the velocity of the particle before it begins to be slowed down by interaction with the wall. The data shows a strong correlation with St and agreement with the theoretical calculations of Davis *et al.* (1986). It demonstrates that the effect of the interstitial fluid causes a decrease in the coefficient of restitution with decreasing Stokes number and that there is a critical Stokes number of about 8 below which particles do not rebound but come to rest against the wall. It is also evident in figure 13.10 that some of the data, particularly at low St shows significant scatter. Joseph *et al.* were able to show that the magnitude of the scatter depended on the relation between the size of the typical asperities on the surface of the particles and the estimated minimum thickness of the film of liquid separating the particle and the wall. When the former exceeded the latter, large scatter was understandably observed. Joseph (2003) also accumulated data for oblique collisions that appear to manifest essentially

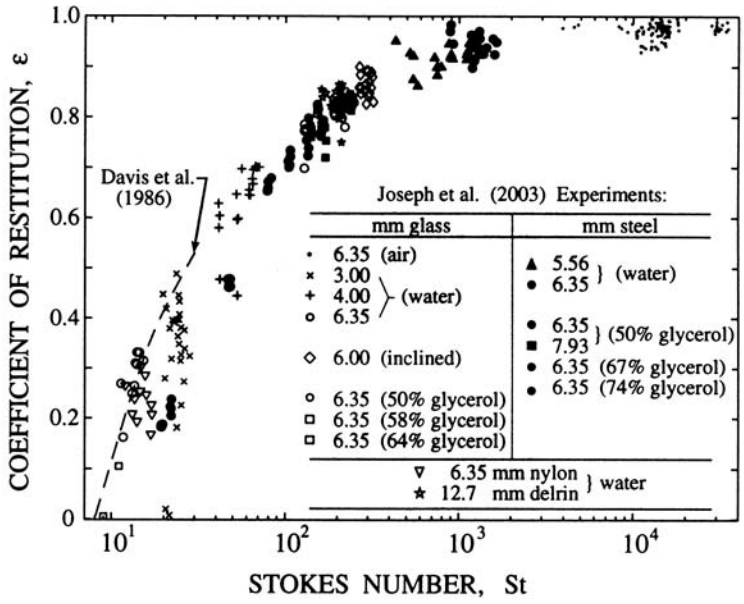

Figure 13.10. Coefficients of restitution for single particles colliding normally with a thick Zerodur wall. The particles are spheres of various diameters and materials suspended in air, water and water/glycerol mixtures. The experimental data of Joseph *et al.* (2001) is plotted versus the Stokes number, *St*. Also shown are the theoretical predictions of Davis *et al.* (1986).

the same dependence of the coefficient of restitution on the Stokes number (based on the normal approach velocity, V) as the normal collisions. He also observed characteristics of the tangential interaction that are similar to those elucidated by Maw *et al.*(1976, 1981) for dry collisions.

Parenthetically, we note that the above descriptions of particle-particle and particle-wall interactions with interstitial fluid effects were restricted to large Stokes numbers and would allow the adaptation of kinetic theory results and simulations to those circumstances in which the interstitial fluid effects are small. However, at lower Stokes and Reynolds number, the interstitial fluid effects are no longer small and the particle interactions extend over greater distances. Even, though the particles no longer touch in this regime, their interactions create a more complex multiphase flow, the flow of a concentrated suspension that is challenging to analyze (Sangani *et al.* 1996). Computer simulations have been effectively used to model this rheology (see, for example, Brady 2001) and it is interesting to note that the concept of granular temperature also has value in this regime.

13.6.3 Classes of interstitial fluid effects

We should observe at this point that there clearly several classes of interstitial fluid effects in the dynamics of granular flows. One class of interstitial fluid effect involves a global bulk motion of the interstitial fluid relative to the granular material; these flows are similar to the flow in a porous medium (though one that may be deforming). An example is the flow that is driven through a packed bed in the saltation flow regime of slurry flow in a pipe (see section 8.2.3). Because of a broad data base of porous media flows, these global flow effects tend to be easier to understand and model though they can still yield unexpected results. An interesting example of unexpected results is the flow in a vertical standpipe (Ginestra *et al.* 1980).

Subtler effects occur when there is no such global relative flow, but there are still interstitial fluid effects on the random particle motions and on the direct particle-particle interactions. One such effect is the transition from inertially-dominated to viscously-dominated shear flow originally investigated by Bagnold (1954) and characterized by a critical Bagnold number, a phenomena that must still occur despite the criticism of Bagnold's rheological results by Hunt *et al.*(2002). We note a similar transition has been observed to occur in hopper flows, where Zeininger and Brennen (1985) found that the onset of viscous interstitial fluid effects occurred at a consistent critical Bagnold number based on the extensional deformation rate rather than the shear rate.

Consequently, though most of these subtler interstitial fluid effects remain to be fully explored and understood, there are experimental results that provide some guidance, albeit contradictory at times. For example, Savage and McKeown (1983) and Hanes and Inman (1985) both report shear cell experiments with particles in water and find a transition from inertially-dominated flow to viscous-dominated flow. Though Hanes and Inman observed behavior similar to Bagnold's experiments, Savage and McKeown found substantial discrepancies.

Several efforts have been made to develop kinetic theory models that incorporate interstitial fluid effects. Tsao and Koch (1995) and Sangani *et al.*(1996) have explored theoretical kinetic theories and simulations in the limit of very small Reynolds number ($\rho_C \dot{\gamma} D^2/\mu_C \ll 1$) and moderate Stokes number ($m_p \dot{\gamma}/3\pi D\mu_C$ - note that if, as expected, V is given roughly by $\dot{\gamma}D$ then this is similar to the Stokes number, St, used in section 13.6.2). They evaluate an additional contribution to Γ, the dissipation in equation 13.13, due to the viscous effects of the interstitial fluid. This supplements the collisional contribution given by a relation similar to equation 13.16. The

problem is that flows with such Reynolds numbers and Stokes numbers are very rare. Very small Reynolds numbers and finite Stokes numbers require a large ratio of the particle density to the fluid density and therefore apply only to gas-solids suspensions. Gas-solids flows with very low Reynolds numbers are rare. Most dense suspension flows occur at higher Reynolds numbers where the interstitial fluid flow is complex and often turbulent. Consequently one must face the issues of the effect of the turbulent fluid motions on the particle motion and granular temperature and, conversely, the effect those particle motions have on the interstitial fluid turbulence. When there is substantial mean motion of the interstitial fluid through the granular material, as in a fluidized bed, that mean motion can cause considerable random motion of the particles coupled with substantial turbulence in the fluid. Zenit *et al.* (1997) have measured the granular temperature generated in such a flow; as expected this temperature is a strong function of the solids fraction, increasing from low levels at low solids fractions to a maximum and then decreasing again to zero at the maximum solids fraction, α_m (see section 14.3.2). The granular temperature is also a function of the density ratio, ρ_C/ρ_D. Interestingly, Zenit *et al.* find that the granular temperature sensed at the containing wall has two components, one due to direct particle-wall collisions and the other a radiative component generated by particle-particle collisions within the bulk of the bed.